



Cite this: *Nanoscale Adv.*, 2021, **3**, 1515

## Recent progress in two-dimensional materials for terahertz protection

Jialiang Pan,<sup>ab</sup> Haowen Hu,<sup>a</sup> Zechen Li,<sup>a</sup> Jingyang Mu,<sup>b</sup> Yunxiang Cai<sup>b</sup> and Hongwei Zhu <sup>\*a</sup>

With the wide applications of terahertz (THz) devices in future communication technology, THz protection materials are essential to overcome potential threats. Recently, THz metamaterials (MMs) based on two-dimensional (2D) materials (e.g., graphene, MXenes) have been extensively investigated due to their unique THz response properties. In this review, THz protection theories are briefly presented first, including reflection loss and shielding mechanisms. Then, the research progress of graphene and other 2D material-based THz MMs and intrinsic materials are reviewed. MMs absorbers in the forms of single layer, multiple layers, hybrid and tunable metasurfaces show excellent THz absorbing performance. These studies provide a sufficient theoretical and practical basis for THz protection, and superior properties promised the wide application prospects of 2D MMs. Three-dimensional intrinsic THz absorbing materials based on porous and ordered 2D materials also show exceptional THz protection performance and effectively integrate the advantages of intrinsic properties and the structural characteristics of 2D materials. These special structures can optimize the surface impedance matching and enable multiple THz scatterings and electric transmission loss, which can realize high-efficiency absorption loss and active controllable protection performance in ultra-wide THz wavebands. Finally, the advantages and existing problems of current THz protection materials are summarized, and their possible future development and applications are prospected.

Received 15th December 2020  
Accepted 28th January 2021

DOI: 10.1039/d0na01046d  
[rsc.li/nanoscale-advances](http://rsc.li/nanoscale-advances)

### 1. Introduction

As most promising waveband for next generation communication (6G) applications, THz waves have attracted extensive attention.<sup>1–4</sup> However, due to potential threats of this unknown waveband to human health, electromagnetic interference, information security and military stealth, essential THz protection materials should be fully studied before their large-

<sup>a</sup>State Key Lab of New Ceramics and Fine Processing, School of Materials Science and Engineering, Tsinghua University, Beijing 100084, China. E-mail: hongweizhu@tsinghua.edu.cn

<sup>b</sup>The First Scientific Research Institute of Wuxi, Wuxi 214035, Jiangsu, China



Jialiang Pan is a PhD candidate at the School of Materials Science and Engineering, Tsinghua University, China. He works as an Engineer (2007–present) at the First Scientific Research Institute of Wuxi, China. His current research interests focus on materials with nano-structures for electromagnetic applications.



Haowen Hu is a PhD candidate at the School of Materials Science and Engineering, Tsinghua University, China. He received his B.S. degree in Materials Science and Engineering (2015) from Beihang University and his Master's degree in Polymer Materials Science and Engineering (2016) from the University of Manchester. He is currently working on 2D semiconductor materials and micro-nano electronic devices.



scale application. To achieve effective reflection loss or transmission shielding of the surplus THz energy, the THz protection materials are mainly THz absorbing and shielding materials. From the point of view of the interaction between electromagnetic (EM) waves and materials, the response mechanism of natural materials is not continuous across the whole spectrum. Within wavebands of hundreds of gigahertz, electrons dominate the response process to EM waves. Moreover, in the infrared to ultraviolet waveband, the EM waves mainly interact with photons of the materials. However, between the two response areas, the 0.1–10 THz band is a “terahertz gap” which lacks material response; therefore, it is an important topic to develop effective THz protection materials.<sup>5,6</sup>

Two-dimensional (2D) materials such as graphene and MXenes, due to their high conductivity, ultra-thickness, large specific surface area, ultra-light weight, high strength and adjustable electromagnetic response, have shown excellent microwave attenuation performance,<sup>7–9</sup> which has encouraged researchers to realize their THz protection abilities.<sup>10–13</sup> However, single atomic layered 2D materials cannot absorb the incident THz energy effectively, and simply stacked materials lead to impedance mismatching.<sup>14,15</sup> Therefore, in order to make full use of the advantages of 2D materials, it is very important to reasonably design the forms of 2D materials in THz protective materials, such as patterning the resonance units of MM absorbers and forming nanostructured materials.<sup>13,16–18</sup> Because MMs have been proved to respond to THz radiation<sup>5</sup> and fully absorb microwave energy,<sup>19,20</sup> THz MMs have potential to be perfect THz absorbers. MMs are artificial EM dielectric materials, and are usually composed of an MM layer (high-conductivity materials with periodically repeated patterns), a dielectric spacer and a metal ground layer. Electrons resonated in these subwavelength scale unit structures can form THz absorption;<sup>21</sup> therefore, the THz response of MMs can be controlled by designing the unit structure and component materials. Similar to traditional metal resonant MMs layers,<sup>22–27</sup> coherent and patterned graphene 2D materials applied as MM layers have been widely studied because of their high conductivities and unique EM responses (such as Surface Plasmon

Polaritons (SPPs)).<sup>17,18,28–30</sup> Otherwise, for the single atomic layer thickness and tunable chemical potential, 2D materials are easy to composite with other materials, and their EM properties can be controlled by external stimuli. Recently, by optimizing the composite structures and active control approaches of MMs, many THz protection MMs with wide response bands and adjustable absorption performance have been designed.<sup>20,31,32</sup>

In addition to 2D materials-based THz protection MMs, the nanostructured 2D materials are effective THz protection materials in the form of intrinsic loss.<sup>10,16,33</sup> The enhanced absorption of nanostructured materials is mainly contributed by their porous structures and long-distance conductive networks. On the one hand, the porous structure ensures proper effective permittivity, which gives a good impedance match to reduce the surface reflection. On the other hand, the cross-linked 2D materials can generate large surface-induced current, so that the THz radiation rapidly decays and turns into heat in the resistance network. Furthermore, by compositing the nanostructured 2D materials with other THz loss materials, the THz response properties would be further regulated to achieve a wider effective waveband and stronger attenuation capability.<sup>16</sup>

In this Review, we focus on recent progress in THz protection materials based on 2D materials, including THz protection MMs and intrinsic loss materials, as shown in Fig. 1. The 2D materials discussed here are mainly graphene and MXenes, along with phosphorene and other 2D materials. Firstly, the THz protection theories are briefly presented, including reflection loss and shielding mechanisms. Secondly, the research progress of graphene and other 2D materials-based THz protection MMs and intrinsic materials is reviewed. Finally, the advantages and existing problems of current THz protection materials are summarized, and their future development and applications are prospected.

## 2. THz protection theory

For different applications, THz protection materials should show different properties. In many cases, the THz protection



*Zechen Li is a PhD candidate at the School of Materials Science and Engineering, Tsinghua University, China. He received his B.S. degree from Tsinghua University in 2019. His research interests focus on the synthesis and structural engineering of nanomaterials for photoelectric detection.*



*Hongwei Zhu is a Professor of School of Materials Science and Engineering, Tsinghua University, China. He received his B.S. degree in Mechanical Engineering (1998) and his PhD degree in Materials Processing Engineering (2003) from Tsinghua University. After postdoctoral studies in Japan and the USA, he began his independent career as a faculty member at Tsinghua University (2008–present). His current research interests involve low-dimensional materials and materials informatics.*



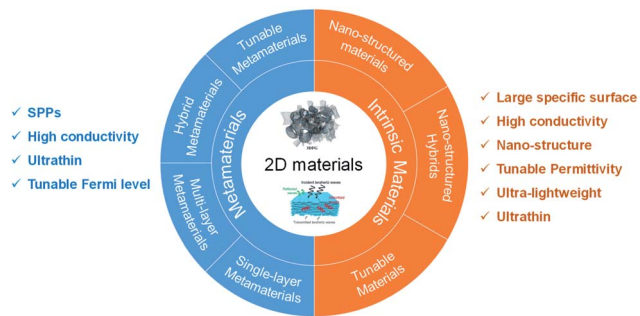


Fig. 1 Schematic of THz protection materials based on 2D materials.

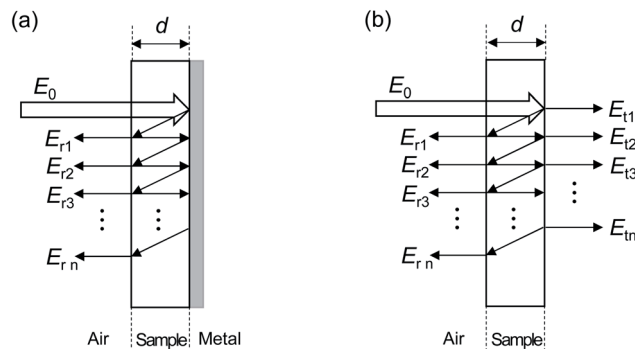


Fig. 2 Schematic models of (a) THz reflection loss and (b) THz shielding theories.

materials must efficiently absorb THz radiation to reduce the THz echo as much as possible and form reflection loss. In some other cases, the THz transmittance must be strictly low, which can shield the incident THz radiation. The two THz protection theories are briefly presented as follows.

## 2.1 THz reflection loss

According to electromagnetic transmission theory, a simplified transmission model of THz reflection loss can be established, as shown in Fig. 2a.<sup>34,35</sup> The incident THz radiation  $E_0$  is transmitted into the absorbing material from the air. The absorbing material is an infinite flat plate with a thickness of  $d$ , which is covered with a total reflection metal plate on the back.  $E_{r1}$ ,  $E_{r2}$  to  $E_{rn}$  represent the THz radiation intensity of the first reflection and the second reflection until the  $n$ -th reflection, respectively, which are formed after multiple reflections of incident THz through the metal back plate and absorbing material surface. The

$$R = \frac{P_R}{P_0} = \lim_{n \rightarrow \infty} \frac{E_r^2(\omega)}{E_0^2(\omega)}$$

$$= \frac{\{[n(\omega) - 1]^2 + \kappa^2(\omega)\}^2}{\{[n(\omega) + 1]^2 + \kappa^2(\omega)\}^2} + 16 \frac{n^2(\omega) + \kappa^2(\omega)}{\{[n(\omega) + 1]^2 + \kappa^2(\omega)\}^2} \times$$

accumulation of multiple reflection energies forms the total reflection.

When the THz radiation is normally incident to medium 2 (absorbing material) from medium 1 (air), according to the Fresnel formula, the reflectivity  $R$  and transmittance  $T$  at the interface can be expressed as follows:<sup>35-37</sup>

$$R_{12} = \frac{\tilde{n}_2 - \tilde{n}_1}{\tilde{n}_1 + \tilde{n}_2} \quad (1)$$

$$T_{12} = \frac{2\tilde{n}_1}{\tilde{n}_1 + \tilde{n}_2} \quad (2)$$

$$R_{21} = \frac{\tilde{n}_1 - \tilde{n}_2}{\tilde{n}_1 + \tilde{n}_2} \quad (3)$$

$$T_{21} = \frac{2\tilde{n}_2}{\tilde{n}_1 + \tilde{n}_2} \quad (4)$$

where  $\tilde{n}_1$  and  $\tilde{n}_2$  are the complex refractive indices of medium 1 and medium 2, respectively. For a lossy medium,  $\tilde{n} = n - \kappa i$ , where  $n$  and  $\kappa$  represent the real and imaginary parts of the refractive index, respectively.

The THz wave is attenuated with propagating a certain distance  $L$  in the lossy medium, so the intensity of THz radiation  $E_L(\omega)$  can be expressed as follows:<sup>35</sup>

$$E_L(\omega) = E_0(\omega) \times e^{-i\tilde{n}(\omega)L/c} \quad (5)$$

where  $c$  is the speed of light ( $3 \times 10^{-8} \text{ m s}^{-1}$ ),  $\omega$  is the angular frequency ( $\text{rad s}^{-1}$ ), and  $E_0(\omega)$  is the initial THz signal intensity. The propagation loss  $P_{\tilde{n}}(\omega, L)$ , which is defined as the power ratio of the THz signal after a propagation length to the initial THz signal, can be expressed as follows:<sup>35</sup>

$$P_{\tilde{n}}(\omega, L) = e^{-i\tilde{n}(\omega)L/c} \quad (6)$$

In this case, the total THz energy reflected by the absorbing material can be expressed as follows:<sup>34,35</sup>

$$E_r^2(\omega) = E_{r1}^2(\omega) + E_{r2}^2(\omega) + E_{r3}^2(\omega) + \dots + E_{rn}^2(\omega) = E_0^2(\omega) \times R_{12}^2 + E_0^2(\omega) \times T_{12}^2 \times R_{21}^2 \times P_{\tilde{n}}^4(\omega, L) + E_0^2(\omega) \times T_{12}^2 \times T_{21}^2 \times R_{21}^2 \times P_{\tilde{n}}^8(\omega, L) + \dots + E_0^2(\omega) \times T_{12}^2 \times T_{21}^2 \times R_{21}^{2n-4} \times P_{\tilde{n}}^{4n-4}(\omega, L) \quad (7)$$

The whole reflectivity ( $R$ ), which represents the ratio of the total reflected power ( $P_R$ ) to incident power ( $P_0$ ), can be expressed as follows:<sup>35-37</sup>

$$R = \frac{[n^2(\omega) + \kappa^2(\omega) - 1]^2 \times \exp\left(\frac{-4\omega \times \kappa(\omega) \times d}{c}\right)}{\{[n(\omega) + 1]^2 + \kappa^2(\omega)\} - \{[n(\omega) - 1]^2 + \kappa^2(\omega)\} \times \exp\left(\frac{-4\omega \times \kappa(\omega) \times d}{c}\right)} \quad (8)$$



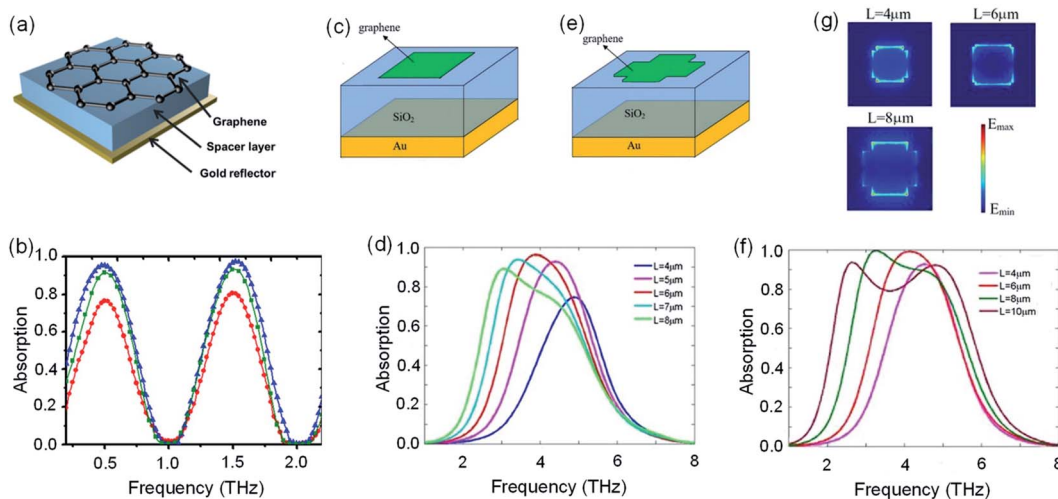


Fig. 3 (a) Diagram of graphene-based Salisbury screen MMs. (b) THz absorption of the MMs illustrated in (a) with different square resistances (sample A: 1295  $\Omega \square^{-1}$  (●), sample B: 817  $\Omega \square^{-1}$  (■), and sample C: 689  $\Omega \square^{-1}$  (▲)) (reproduced with permission from ref. 56. Copyright 2014 AIP Publishing). (c) Unit cell of MMs with the rectangular array. (d) THz absorption of the MMs illustrated in (c) for various values of length L. (e) Unit cell of MMs with the cross-shaped array. (f) THz absorption of the MMs illustrated in (e) for various values of length L. (g) Electric field distributions of the MMs illustrated in (e) at the absorption peak for different values of L (reproduced with permission from ref. 59. Copyright 2017 The Optical Society).

Therefore, the reflection loss ( $R_L$ ) can be written in decibels (dB) as follows:<sup>16,34,35</sup>

$$R_L = -10 \times \lg \left[ \lim_{n \rightarrow \infty} \frac{E_r^2(\omega)}{E_0^2(\omega)} \right] \quad (9)$$

## 2.2 THz shielding

Similar to the THz reflection loss, a THz shielding model was built with a slight difference, as shown in Fig. 2b.<sup>34</sup> The THz shielding material is also an infinite flat plate, but without a metal layer on the back. Therefore, in addition to multiple

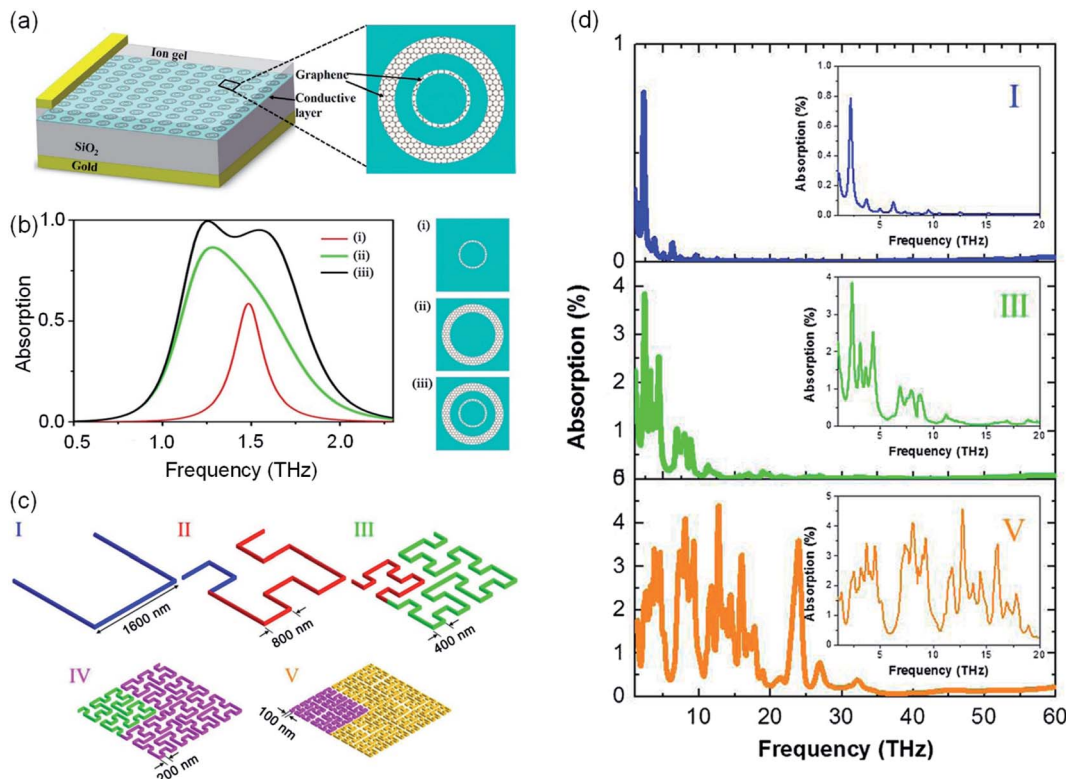


Fig. 4 (a) Schematic of the THz absorber consisting of the GCDR. (b) Simulated absorptions of the proposed GCDR absorber with different graphene patterns (reproduced with permission from ref. 66 Copyright 2018 The Optical Society). (c) Iterative construction of the Hilbert curve for the first five (I–V) levels. (d) Simulated absorptions for graphene Hilbert structures of levels I, III, and V (reproduced with permission from ref. 69 Copyright 2016 American Physical Society).



reflections, there are corresponding THz transmission waves, labeled as  $E_{t1}$ ,  $E_{t2}$  to  $E_{tn}$ .

Accordingly, the total THz transmission of the shielding material can be expressed as the sum of all multiple transmission energies:<sup>34,36</sup>

$$\begin{aligned} E_t^2(\omega) &= E_{t1}^2(\omega) + E_{t2}^2(\omega) + E_{t3}^2(\omega) + \dots, \\ + E_{tn}^2(\omega) &= E_0^2(\omega) \times T_{12}^2 \times T_{21}^2 \times P_n^2(\omega, L) \\ + E_0^2(\omega) \times T_{12}^2 \times T_{21}^2 \times R_{21}^4 &\times P_n^6(\omega, L) \\ + E_0^2(\omega) \times T_{12}^2 \times T_{21}^2 \times R_{21}^8 &\times P_n^{10}(\omega, L) + \dots, \\ + E_0^2(\omega) \times T_{12}^2 \times T_{21}^2 \times R_{21}^{4n-4} &\times P_n^{4n-2}(\omega, L) \end{aligned} \quad (10)$$

Thus, the whole THz transmittance ( $T$ ) can be written by the total transmitted power ( $P_T$ ) and the incident power ( $P_0$ ).<sup>34,36</sup>

$$T = \frac{P_T}{P_0} = \lim_{n \rightarrow \infty} \frac{E_t^2(\omega)}{E_0^2(\omega)} = 16 \times \frac{[n^2(\omega) + \kappa^2(\omega)] \times \exp\left(\frac{-2\omega \times \kappa(\omega) \times d}{c}\right)}{\{[n(\omega) + 1]^2 + \kappa^2(\omega)\}^2 - \{[n(\omega) - 1]^2 + \kappa^2(\omega)\}^2 \times \exp\left(\frac{-4\omega \times \kappa(\omega) \times d}{c}\right)} \quad (11)$$

Therefore, the electromagnetic shielding effectiveness (EMI SE) can be written in dB as follows:<sup>16,34,35</sup>

$$\text{EMISE} = -10 \times \lg \left[ \lim_{n \rightarrow \infty} \frac{E_t^2(\omega)}{E_0^2(\omega)} \right] \quad (12)$$

### 3. Graphene-based THz protection materials

#### 3.1 Graphene-based THz protection MMs

**3.1.1 Single-layer graphene MMs.** Because of the obvious SPPs in the THz band,<sup>30</sup> graphene has been widely studied for

THz protection.<sup>38–54</sup> However, atomic monolayer graphene is almost transparent to THz waves; thus, the overall intrinsic absorption of monolayer graphene is highly limited.<sup>14,15</sup> Therefore, originating from the SPPs effect, well-designed continuous or patterned graphene in the MMs layer can generate collective oscillation of the charge density and light on the interface between graphene and its surroundings, which is beneficial to effective THz absorption and protection.<sup>39</sup> The THz response of continuous films was extensively studied, which is promising for further application in THz protection.<sup>17,43,55,56</sup> By using polymethyl methacrylate (PMMA), Min *et al.*<sup>56</sup> transferred a continuous 2D graphene sheet grown on nickel to a polymer substrate with a gold-bottomed film. The whole structure built up a Salisbury screen MM, as shown in Fig. 3a, in which the

graphene sheet worked as the resistance layer. The conductivity of the graphene sheet could be regulated by chemical doping to match the free space impedance; therefore, the incident THz attenuated directly in the MMs by way of destructive interference. The measured results showed that when the square resistance of the graphene sheet was  $689 \Omega \cdot \square^{-1}$ , maximum absorptions of 0.95 and 0.97 could be achieved at 0.97 and 1.5 THz (Fig. 3b). In addition, some patterned graphene, such as square,<sup>38,57</sup> cross,<sup>58–61</sup> disk,<sup>60,62</sup> ribbon,<sup>63,64</sup> ring<sup>39,65,66</sup> and pixel<sup>67</sup> shapes, have been designed and simulated for THz absorption. Xiao *et al.*<sup>59</sup> designed rectangular and cross-shaped graphene metasurfaces for THz absorption (Fig. 3c and e). The full-wave

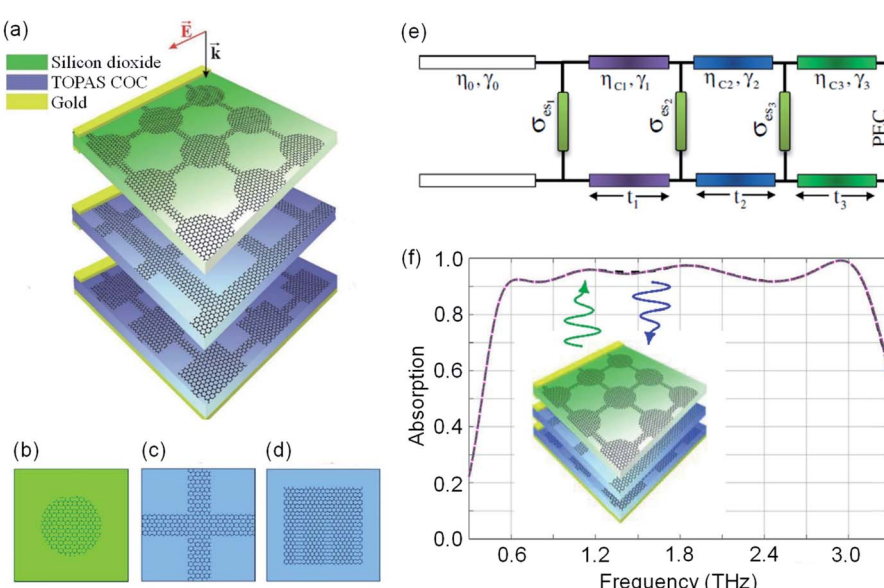


Fig. 5 (a-d) Structure, (e) transmission line model and (f) simulated absorption of multiple-layer graphene MMs (reproduced with permission from ref. 15 Copyright 2018 The Optical Society).



simulation showed that both MMs indicated effective absorbing ability, and the effective absorption (absorption above 90%) bandwidth of the cross-shaped MMs could reach 1.13 THz (Fig. 3d and f). Furthermore, generated from the higher real part conductivity of graphene surface and larger propagation loss of the SPPs, the absorbing range in the low-frequency region was broadened. As shown in Fig. 3g, the electric field distribution at the absorption peak revealed that the localization fields on the edges of the patterned graphene were obviously stronger because of the charge accumulation excited by the electric dipole resonances.

Meanwhile, some complex or composite graphene patterns were proposed to enhance THz absorption<sup>39,60,66,68,69</sup> so that the absorbing bandwidth could be broadened by the multiple resonant peaks generated from the multi-structures. Mou *et al.*<sup>66</sup> designed a patterned graphene concentric double rings (GCDR) metasurface to enlarge the absorbing bandwidth by forming plasmonic hybridization between two graphene rings (Fig. 4a). The calculated absorption results shown in Fig. 4b revealed that the MMs with GCDR can effectively absorb THz energy above 90% ranging from 1.18 to 1.64 THz, with two isolated absorption peaks located at 1.26 and 1.54 THz. Meanwhile, the MMs with only inner or outer graphene single rings exhibited single absorption peaks and narrow bandwidths, corresponding to the high-frequency and low-frequency peaks

of the GCDR structures. The coupling effect between the two graphene rings obviously enhanced the THz absorption, with stronger dissipating ability and wider bandwidth. Moreover, to further broaden the absorption bandwidth, Wu *et al.*<sup>69</sup> proposed broadband MMs based on the self-affine fractal Hilbert curves, in which the self-affine multi-scale structures could induce different resonant frequencies, and the first five (I–V) iterative levels of the Hilbert curves are shown in Fig. 4c. As shown in Fig. 4d, with the increment of the Hilbert curve level, the responsive absorption bandwidth was clearly broadened for the multiple resonant behaviors, which originated from the self-affine structures.

**3.1.2 Multi-layer graphene MMs.** Multi-layer graphene MMs were also commonly introduced to achieve broadband THz protection. The resonant frequencies and coupling effects can be manipulated by designing the graphene patterns of each metasurface to enable the multi-layer graphene MMs to respond to more frequencies and wider THz bandwidths.<sup>15,28,70–78</sup> Rahmanzadeh *et al.*<sup>15</sup> designed the three-layer MMs composed of different graphene metasurfaces with square, cross and circle-shaped patterns, respectively. The multi-layer structures and graphene patterns of each layer are shown in Fig. 5a–d. According to the equivalent circuit model, the patterned graphene layers could be simulated as the dispersion complex impedances (Fig. 5e), in which the

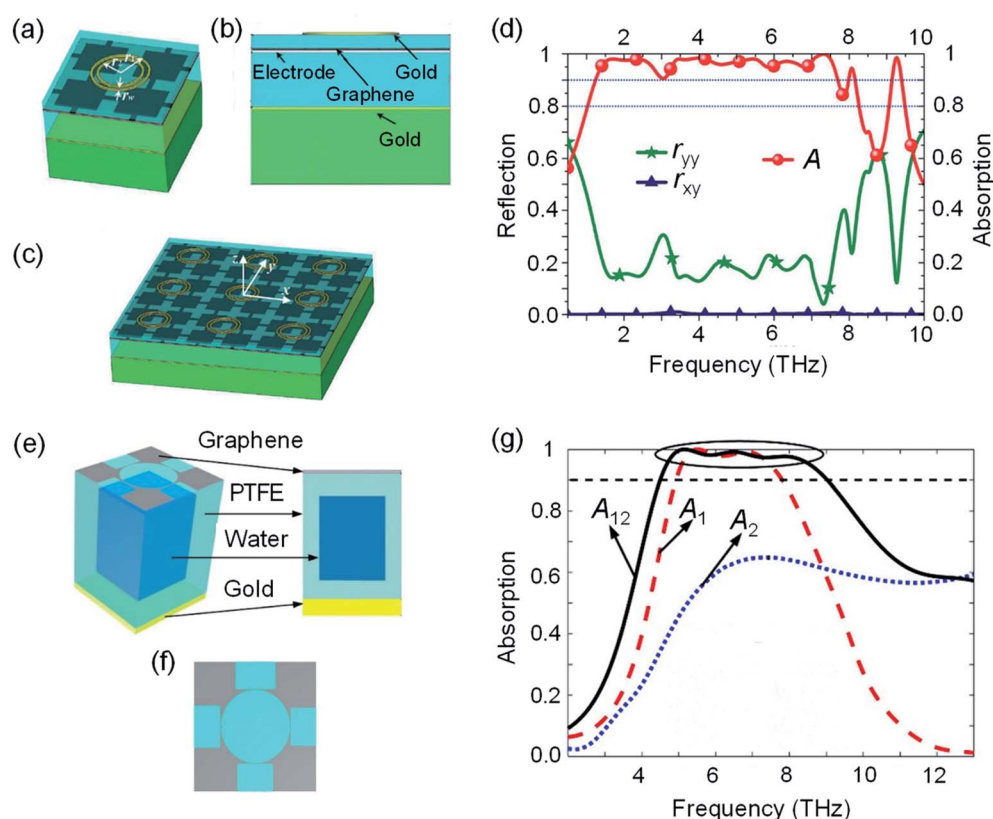


Fig. 6 (a–c) Schematic view of a graphene–metal MMs THz absorber. (d) Simulated THz absorption and reflection of graphene–metal MMs (reproduced with permission from ref. 85 Copyright 2019 The Royal Society of Chemistry). (e and f) Schematic view of a graphene–water MMs THz absorber. (g) Simulated THz absorption of graphene–water MMs (A<sub>12</sub>: graphene–water hybrid MMs, A<sub>1</sub>: A<sub>12</sub> MMs without water, A<sub>2</sub>: A<sub>12</sub> MMs without the patterned graphene metasurface) (reproduced with permission from ref. 94 Copyright 2020 Elsevier).



structural parameters could be theoretically designed for the optimal absorption performance. The THz absorption results of the full-wave simulation shown in Fig. 5f revealed that the multi-layer graphene MMs achieved ultra-wide effective bandwidth, ranging from 0.55 to 3.12 THz. By analyzing the induced electric field, surface current and power loss density of each patterned graphene metasurface, it was clear that the SPPs played a dominant role in the THz dissipation process and formed the physical absorption mechanism of the multi-layer graphene MMs. Meanwhile, the simulation results also verified that the designed structure was omnidirectional and polarization insensitive; therefore, the MMs could effectively protect the device under multi-polarization THz incidences from wide incident angles.

**3.1.3 Hybrid graphene MMs.** In order to further expand the THz response bandwidth and strengthen the THz absorption capability of THz protection materials, it is also effective to combine graphene with other THz responsive materials, such as

metals,<sup>18,79–88</sup> Si,<sup>89–93</sup> water<sup>94</sup> and other materials.<sup>95,96</sup> By reasonably designing the meta-structures of each component, the comprehensive advantages of each material can be utilized. Peng *et al.*<sup>85</sup> designed the hybrid MMs based on four graphene fishing net structures and double metal rings (Fig. 6a–c). As the simulated results show in Fig. 6d, the effective absorption bandwidth of the graphene–metal hybrid MMs could reach as high as 6.46 THz (1.24–7.70 THz). Meanwhile, the absorber was insensitive to different polarizations and incident angles of the THz incidence. The ultra-wide effective THz absorption bandwidth of the graphene–metal hybrid MMs was formed by the following three factors: (i) the SPPs of the graphene metasurface were enhanced by the metal metasurface, leading to the enhancement of the confined field. (ii) The resonance coupling of the metal and graphene metasurface could trap the incident THz wave between the two metasurfaces, which could form energy exchange and dissipation. (iii) The multiple THz reflections and their superposition between the metasurface and gold

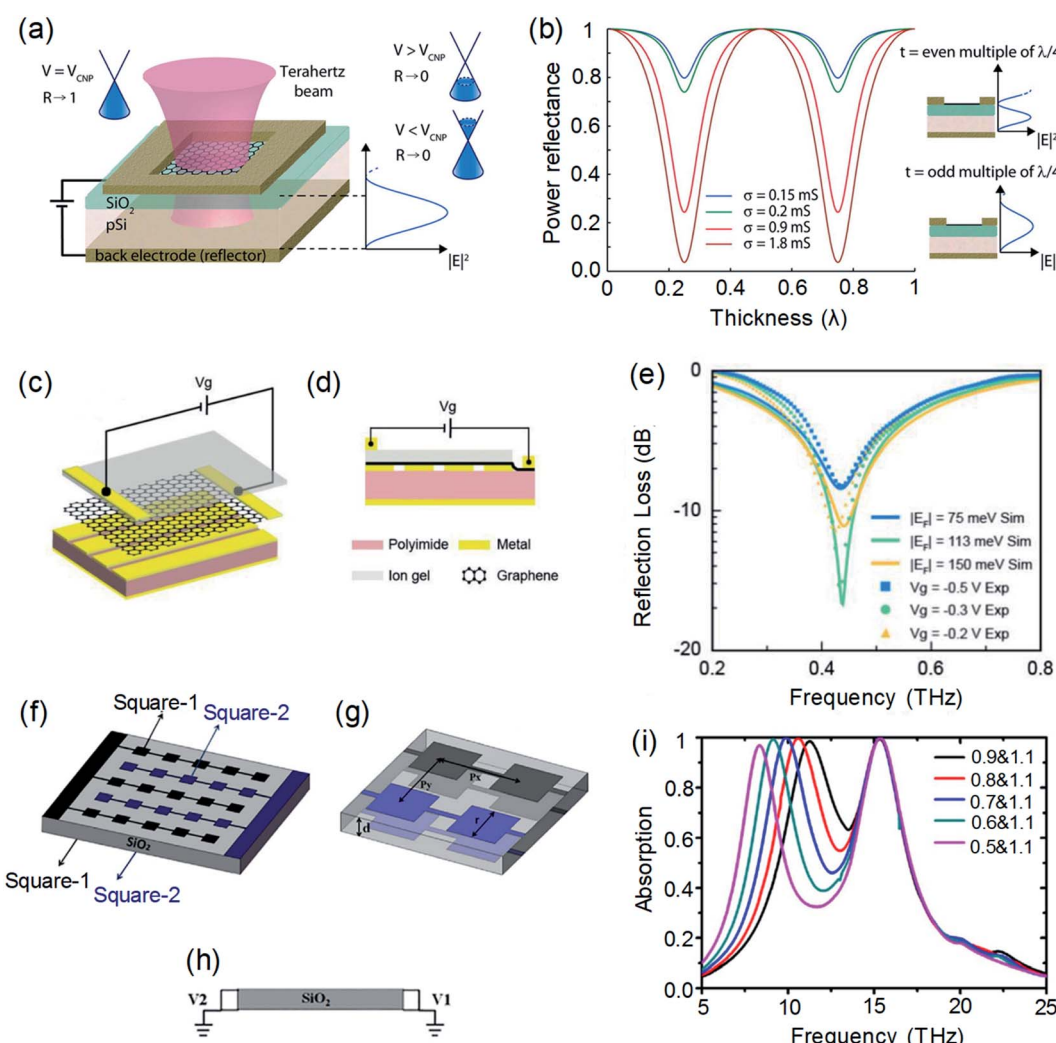


Fig. 7 (a) Schematic structure, operating principle and (b) calculated power reflectance of a graphene THz absorption modulator (reproduced with permission from ref. 110 Copyright 2012 American Chemical Society). (c and d) Schematic view and (e) simulated THz reflection of the tunable MMs THz absorber based on graphene film (reproduced with permission from ref. 103 Copyright 2020 John Wiley and Sons). (f–h) Schematic view and (i) simulated THz absorption of the tunable MMs THz absorber based on patterned graphene (reproduced with permission from ref. 104 Copyright 2019 Elsevier).

substrate further enhanced the THz absorption. In addition, the absorption bandwidth could be broadened by composing graphene MMs with water by taking advantage of the intrinsic dispersive permittivity of water. Zhang *et al.*<sup>94</sup> designed a graphene–water hybrid MMs THz absorber with an ultra-wide effective waveband, in which water was encapsulated in the polytetrafluoroethylene (PTFT) dielectric material with the patterned graphene metasurface on the top (Fig. 6e and f). The simulated results shown in Fig. 6g present a broad THz effective bandwidth covering 4.52–9.02 THz. It also could be seen that the broadband absorption was superimposed by three absorption peaks, in which two low-frequency absorption peaks were excited by the graphene metasurface, and the high-frequency peak was induced by the water. Moreover, by introducing the filling water, the absorption bandwidth of the hybrid absorber was obviously increased by 57.34% compared to the absorber without water, while the absorption peak of the graphene metasurface was not shifted. Otherwise, the graphene–water MMs absorber was confirmed to be insensitive to the incident angles and polarizations.

**3.1.4 Tunable graphene MMs.** Because graphene is a typical 2D semiconductor, its electron mobility and Fermi level can be controlled by external stimulations, such as an electrostatic field,<sup>59,90,97–110</sup> magnetic field,<sup>111,112</sup> optical pump<sup>113</sup> and temperature.<sup>83,114</sup> The resonance frequencies of the designed graphene structures can thus be regulated by external stimulation, which can form effective and broadband THz absorption. According to the Kubo formula, the surface conductivity of graphene could be expressed as follows:<sup>103</sup>

$$\sigma_g = i \frac{e^2 K_B T}{\pi \hbar^2 (\omega + i/\tau)} \left[ \frac{E_F}{K_B T} + 2 \ln \left( \exp \left( - \frac{E_F}{K_B T} \right) + 1 \right) \right] + i \frac{e^2}{4\pi\hbar} \ln \left[ \frac{2|E_F| - \hbar(\omega + i/\tau)}{2|E_F| + \hbar(\omega + i/\tau)} \right] \quad (13)$$

where  $K_B$ ,  $e$ ,  $\hbar$ ,  $\tau$ ,  $T$  and  $E_F$  are the Boltzmann constant, electron charge, reduced Planck's constant, relaxation time, temperature and Fermi level, respectively. From the formula, it is obvious that the surface conductivity of graphene can be actively controlled by the Fermi level and temperature. Sensale-Rodriguez *et al.* designed an extraordinary controllable THz modulator by transferring single-layer graphene onto a  $\text{SiO}_2/\text{p-Si}$  substrate (Fig. 7a).<sup>110</sup> The carrier concentration and Fermi level in graphene could be tuned when the voltage employed between the graphene and back metal was changed. While the Fermi level was modulated to the Dirac point ( $V = V_{\text{CNP}}$ ), the THz absorption was at its minimum. Moreover, the THz absorption increased as the Fermi level shifted into the valence or conduction band, due to the intraband transition of the available density of states. The calculated power reflectance in Fig. 1b showed that the field intensity in graphene is maximum when the optical thickness of the substrate is an odd-multiple of the THz wavelength, in which obvious absorption swings occurred when the conductivity in graphene was extraordinarily controlled. However, the THz absorption was very low and did not change when the substrate thickness was an even-multiple of the THz wavelength. Furthermore, by integrating the metal grating into chemical vapor deposition (CVD)-grown graphene sheet Salisbury screen MMs, Chen *et al.*<sup>103</sup> realized an electrically tunable hybrid THz MM absorber based on an ion gel/

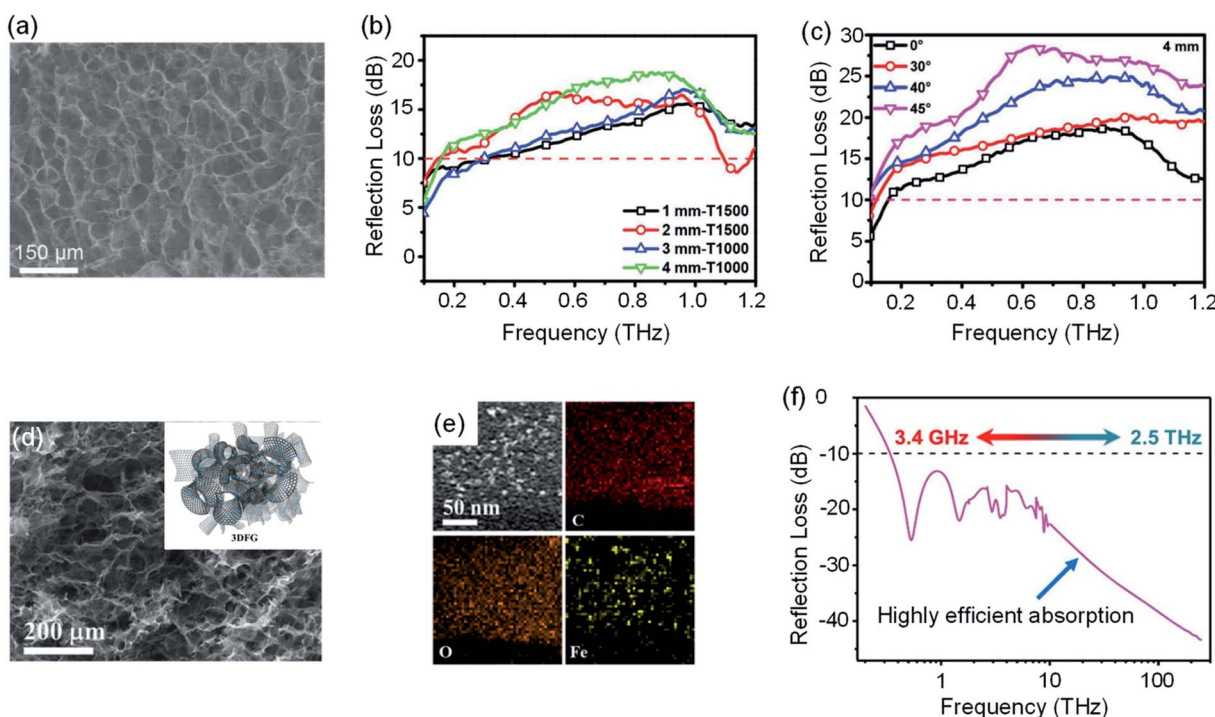


**Fig. 8** (a) Cross-section SEM image of the 3D graphene foams. (b) Reflection loss curves of some graphene foam samples. (c) Reflection loss curves of the T1000 samples with 4 mm thickness at different incident angles (reproduced with permission from ref. 10 Copyright 2018 John Wiley and Sons). (d) SEM image, structural diagram, (e) EDS maps and (f) reflection loss curve of the graphene/Fe<sub>3</sub>O<sub>4</sub> hybrid foams (reproduced with permission from ref. 35 Copyright 2019 American Chemical Society).



graphene/stripe Al/polyimide (PI)/Al thin film structure (Fig. 7c and d). The Fermi level of the graphene layer could be changed by the external bias voltage, which could lead to controllable THz absorbing ability. The experimental results showed that it is feasible to achieve tunable THz absorption based on graphene grown by CVD with low carrier mobility, and the modulation depth of the THz absorption could reach 25% by applying relatively small bias voltage (−2 to 2 V), as shown in Fig. 7e. Then, the numerical simulations based on transmission line theory and full-wave simulation software also verified the measured results. In addition to graphene nanosheets, some patterned graphene structures were also designed and prepared for tunable THz absorption. Jin *et al.*<sup>104</sup> designed a coherent perfect absorber based on the square patterned graphene structure, which was composed of two alternately arranged graphene MM layers (Fig. 7f–h). The Fermi level of each staggered metastructure could be independently controlled by the applied bias voltage distributed on the side. The numerical simulation results showed that the absorbing frequency peaks can be effectively controlled by changing the applied voltage values, and the absorber presented two independent tunable absorption peaks when the applied voltages of each staggered metastructure were different (Fig. 7i). Moreover, when the absorber was stacked by the metastructures in layers, multiple THz absorption peaks could be formed to achieve an ultra-wide THz absorbing waveband. Although the preparation of tunable patterned graphene MMs is currently difficult, it can also be achieved by template selective etching and some other new methods.<sup>101</sup>

### 3.2 Graphene intrinsic THz protection materials

**3.2.1 Graphene foams.** As an advanced carbon material with high thermal conductivity, high strength, large specific surface area, optical transparency and adjustable electromagnetic response, graphene has been widely used in radar wave attenuation and showed excellent loss performance;<sup>7</sup> therefore, its THz protection applications have attracted much attention.<sup>10–12,35</sup> In contrast to the reflection mechanism of traditional metal THz shielding materials, Zdrojek *et al.*<sup>11</sup> prepared flexible THz shielding materials by dispersing graphene nanosheets in a polydimethylsiloxane (PDMS) matrix, whose shielding effect was mainly contributed by absorption. The shielding material showed excellent unit shielding efficiency exceeding  $30 \text{ dB cm}^{-3} \text{ g}^{-1}$ . However, because of their inhomogeneous dispersion and interface mismatch, the THz shielding materials of this type would produce large surface reflections; thus, the maximum absorption hardly reached 80%. Therefore, adjusting the THz characteristics and improving THz attenuation are still challenging.<sup>10</sup> In recent years, with the fabrication development of 3D porous materials, such as graphene foams, THz absorbers with conductive networks and large surface areas can be established which can provide excellent impedance matching and THz energy attenuation.<sup>7,10,35,115</sup> Huang *et al.*<sup>10</sup> prepared a 3D porous graphene foam with a density of only  $0.8 \text{ g cm}^{-3}$  by a solvothermal method (Fig. 8a). The optimal reflection loss of the THz absorber could reach 19 dB at 0.88 THz, and the effective absorbing bandwidth (reflection loss above 10 dB) could cover 95% of the test band (0.1–1.2 THz) under normal conditions, as shown in Fig. 8b. Moreover, when the incident

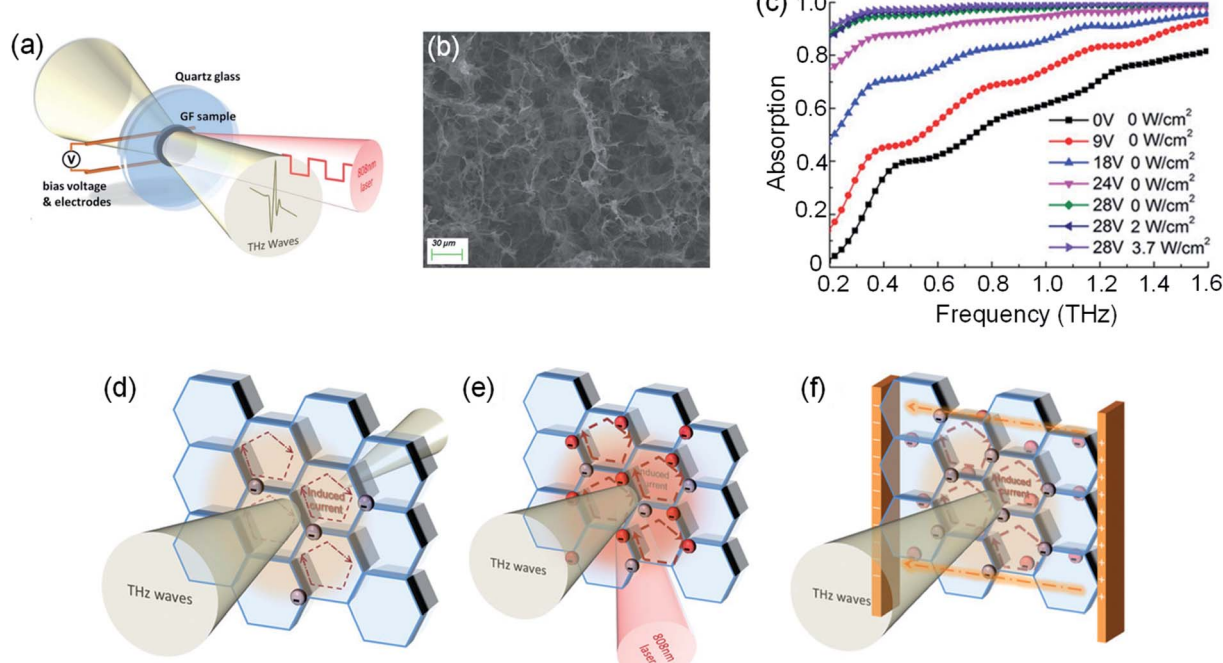


Fig. 9 (a) Schematic of electrically and optically controlled graphene foams for THz modulation and absorption. (b) SEM image of tunable THz absorbing graphene foams. (c) The absorptivity curves of tunable graphene foams stimulated by different electrical voltages and laser excitations. Schematic of THz wave propagation and interaction with free electrons in the graphene foams (d) without external field excitations, (e) excited by the laser light and (f) excited by the electric field (reproduced with permission from ref. 36 Copyright 2019 John Wiley and Sons).



angle was  $45^\circ$ , the effective bandwidth covered the whole test bandwidth, while the optimal reflection loss was 28.6 dB at 0.64 THz (Fig. 8c). It was found that the outstanding THz absorbing ability of 3D graphene foam mainly originates from the porous structure and long distance conductive network. On the one hand, the effective dielectric constant and impedance matching degree can be optimized by designing the porous structures to reduce the surface reflection. On the other hand, the 3D graphene sheets could induce surface currents under the THz radiation so that the incident THz energy would be rapidly decayed in the resistance network by being converted into heat.

**3.2.2 Graphene hybrid foams.** To further enhance the THz protection properties, 3D graphene foams composed with carbon nanotubes,<sup>116</sup>  $\text{Fe}_3\text{O}_4$  (ref. 35) and other dielectric/magnetic particles were proposed to perform multiple attenuation mechanisms. Chen *et al.*<sup>35</sup> prepared high-performance graphene/ $\text{Fe}_3\text{O}_4$  3D porous electromagnetic protection foams with ultra-lightweight and ultra-wide effective wavebands (Fig. 8d and e). The measured results showed that the 3D foams could achieve an effective absorption waveband covering 3.4

GHz to 2.5 THz, while the average reflection loss reached  $-38$  dB (Fig. 8f). In addition, the 3D composite foams exhibited excellent absorption properties under oblique incidence and different compression strains, while the absorber still maintained a stable absorption ability after 200 repeated compression/release cycles. The addition of magnetic particles further regulated the electromagnetic characteristics of the 3D graphene porous cross-linked structures, which greatly broadened the response waveband and provided a strong technological foundation for active protection materials according to the increasingly complex electromagnetic environments in the future.

**3.2.3 Tunable graphene THz protection materials.** In addition, because the Fermi level and carrier concentration of graphene can be conveniently regulated by some external stimuli, such as electric field and optical radiation, THz absorbing modulation of graphene foams is also available. Xu *et al.*<sup>36</sup> studied the active modulation behaviors of an 800 nm laser and bias electric field on graphene foams, and they realized flexible regulation of THz shielding and

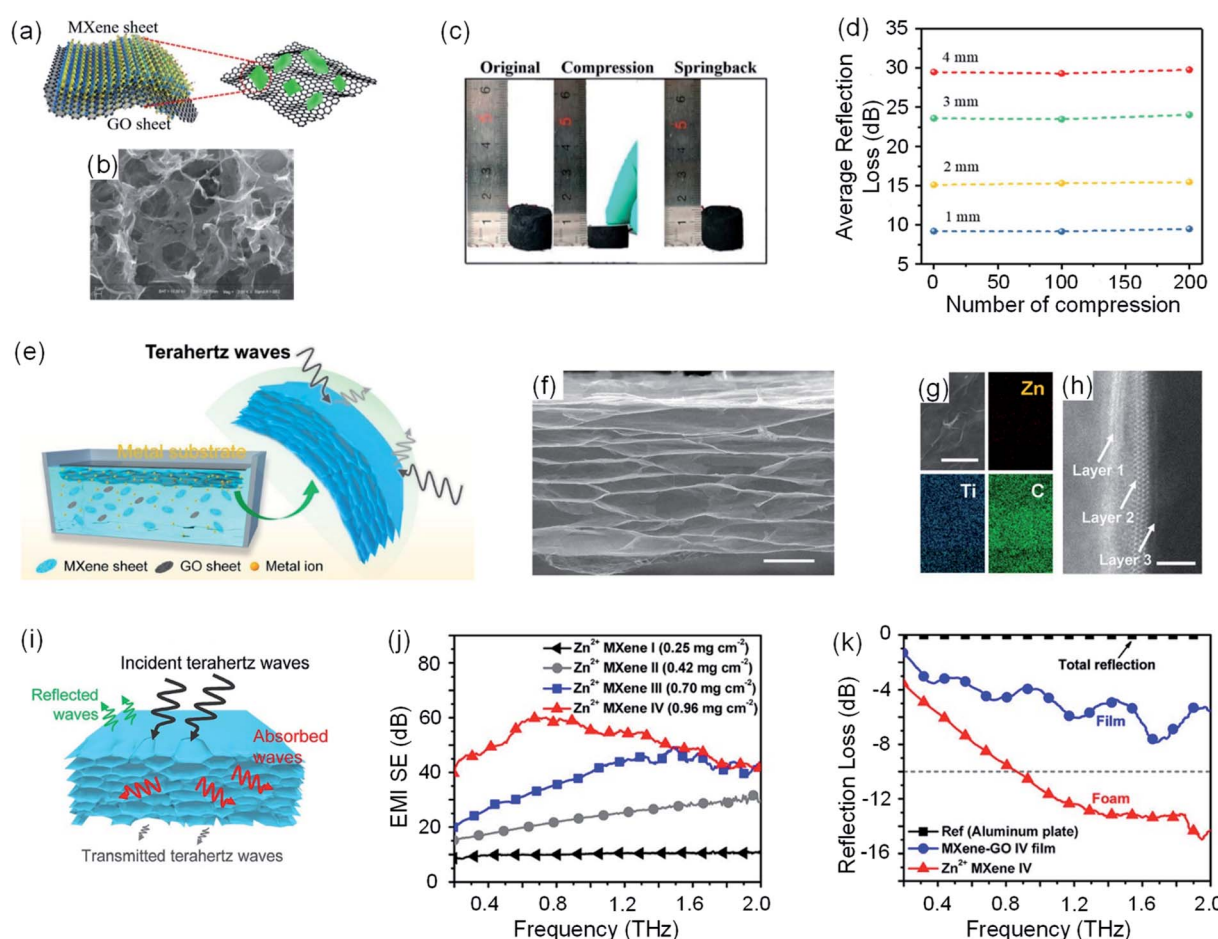


**Fig. 10** (a) Digital images, (b) structural diagram and (c) SEM image of MXene/GO 3D foam. (d) Reflection loss curves of MXene/GO 3D foams with different thicknesses after compression 0, 100 and 200 times (reproduced with permission from ref. 37 Copyright 2019 American Chemical Society). (e) Structural diagram, (f) sectional SEM image, (g) EDS maps, (h) HAADF-STEM image, (i) THz shielding schematic, (j) THz shielding efficiency curves and (k) reflection loss curves of MXene/GO/ $\text{Zn}^{2+}$  composite 3D foams (reproduced with permission from ref. 16 Copyright 2020 American Chemical Society).



absorbing performance. A schematic of the external stimulus control and the microstructures of the graphene foams are shown in Fig. 9a and b. The absorptivity curves shown in Fig. 9c reveal that the THz absorption was strongly related to the frequency when there was no external field, with an absorptivity change from 0.04 at 0.2 THz to 0.8 at 1.6 THz. Furthermore, the absorption increased sharply with the increment of the excitation intensity. The absorptivity changed rapidly from 0.13 to 0.954 at the low frequency of 0.3 THz, while the absorptivity at the high frequency of 1 THz varied from 0.62 to 0.995. The excellent THz absorbing modulation properties can be explained as follows: (i) without external stimulation, the cross-linked graphene networks can be regarded as numerous coupling circuits of resistance, inductance and capacitance; therefore, the time-varying THz field could excite induced currents on the cell wall of graphene. These long-range induced currents attenuated rapidly in the high resistance networks, resulting in sharp decay of the incident THz wave (Fig. 9d). (ii) When the graphene foams were stimulated by a laser or electric field, the nonequilibrium carriers could be generated to raise the Fermi level to a higher conduction band and enhance the THz absorption (Fig. 9e and f). (iii) Fundamentally, because the laser radiation could not penetrate the interior of the graphene foams, the photo-generated carriers could only be generated in the shallow layer of the foams. However, the electric field could pass through the whole graphene foams, resulting in more nonequilibrium carriers on the graphene sheets, which caused a superior regulating effect compared to laser radiation.

## 4. Other 2D THz protection materials

### 4.1 MXene-based intrinsic THz protection materials

In addition to graphene, MXenes have been commonly used as 2D THz protection materials in recent years.<sup>13,16,37,117</sup> MXenes are 2D transition-metal carbide and nitride materials with the general formula  $M_{n+1}X_nT_x$ . MXenes have attracted extensive attention for their unique mechanical, structural, physical and chemical properties, among which the ultra-high conductivity ( $1500 \text{ S cm}^{-1}$ ) and hydrophilic surface endow them with excellent electromagnetic response characteristics and controllable structures.<sup>9,118,119</sup> 2D MXene nanosheets can induce conductance of incident electromagnetic waves between the nanosheets due to their good internal conductivity and particular layer spacing, which has been proved to enhance the electromagnetic absorption effectively.<sup>9,120</sup> Furthermore, Jhon *et al.*<sup>121</sup> theoretically confirmed the intrinsic THz response characteristics of MXenes through first principles. Thus, Ma *et al.*<sup>37</sup> prepared ultra-light and compressible THz-absorbing 3D porous MXene/graphene oxide (GO) foams by a solvothermal method (Fig. 10a–c). The absorber combined the advantages of MXenes and GO, forming tunable and ultra-wideband THz absorption properties. MXene/GO foams showed high THz loss efficiency during the whole test range (0.2–2.0 THz) with the maximum reflection loss of 37 dB at 2 THz. Also, when the mass ratio of MXene and GO was 1 : 5, the absorber presented the maximum average absorption loss of 30.6 dB. Moreover, after compression was repeated 200 times, the THz absorption performance of the composite foams was almost unchanged (Fig. 10d). Similar to graphene foam structures, 3D porous

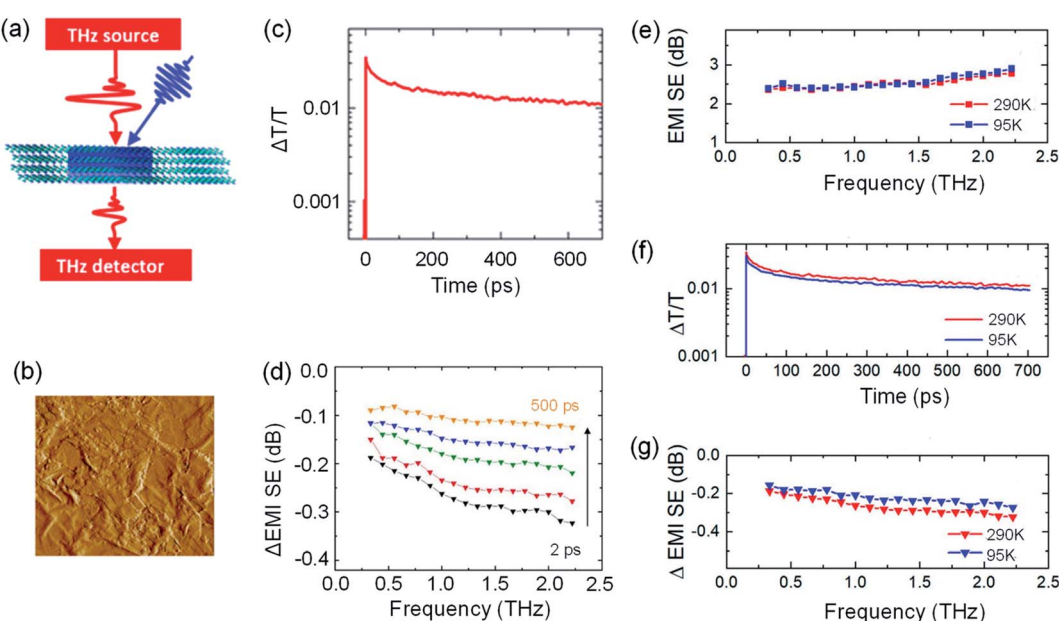


Fig. 11 (a) THz shielding modulation schematic of the MXene film stimulated by optical radiation. (b) AFM micrograph of a 25 nm-thick Ti<sub>3</sub>C<sub>2</sub>T<sub>x</sub> film. (c) THz transmittance and (d) shielding effectiveness changes under different optical radiation times. (e) THz shielding effectiveness of the MXene film at 290 and 95 K without external stimuli. (f) THz transmittance changes after excitation with 800 nm and 950  $\mu\text{J cm}^{-2}$  laser pulses at 290 and 95 K. (g) THz shielding effectiveness changes 2 ps after photoexcitation at 290 and 95 K with 800 nm and 950  $\mu\text{J cm}^{-2}$  pulses (reproduced with permission from ref. 117 Copyright 2020 American Chemical Society).



MXene/GO foams could produce better impedance matching and larger induced current loss, and the introduction of MXenes with high THz response could further improve the THz absorption performance. By utilizing the cross-linking reinforcement of the multivalent metal ions to MXene and GO nanosheets, Lin *et al.*<sup>16</sup> prepared free-standing, lightweight, foldable and highly stable MXene/GO/Zn<sup>2+</sup> THz shielding foams by an ion-diffusion-induced gelation method (Fig. 10e). The measured morphology results showed that a small amount of the Zn component was evenly distributed in the homogenous foams, and the nanosheets were tightly packed in the cell walls of the foams (Fig. 10f-h). The unique cross-linked porous structures and moderate conductivity endowed the foams with higher THz shielding ability and lower surface reflection (Fig. 10i). The THz protection test results showed that when the thickness of the 3D foams was only 85  $\mu$ m, the electromagnetic shielding effectiveness could reach 51 dB, while the reflection loss below  $-10$  dB could cover 0.86–2.0 THz (Fig. 10j and k).

#### 4.2 Tunable MXene-based THz protection materials

Because the electric conductivity of MXenes can be inhibited by external optical stimulation, it is possible to modulate their THz shielding properties. Therefore, Li *et al.*<sup>117</sup> studied the THz shielding regulation of MXene films stimulated by an ultrafast optical pulse (Fig. 11a). Due to the synergistic effects of THz absorption and reflection, the THz shielding effectiveness per unit thickness of the highly conductive Ti<sub>3</sub>C<sub>2</sub>T<sub>y</sub> thin film with

a thickness of only 25 nm (Fig. 11b) could reach  $4 \times 10^5$  dB cm<sup>-2</sup> g<sup>-1</sup>, which indicates that the THz shielding effectiveness of a micron-thickness film could reach tens of decibels. After the stimuli of 400 and 800 nm optical pulses, the transient THz transmittance of the MXene film could be enhanced within 2 ps. The THz shielding was suppressed by the photoinduced transient decrease of the real conductivity components which were proportional to the THz absorption, leading to more THz transmission. Additionally, with increasing irradiation time, the influence on the THz transmittance and shielding gradually weakened (Fig. 11c and d). Moreover, the measured results revealed that the THz shielding effectiveness could be reduced within nanoseconds through ultrafast optical pulses ranging from 95 K to room temperature (Fig. 11e–g). Due to these unique properties, MXenes are promising for the dynamic control of THz shielding and detection devices.

#### 4.3 Other 2D THz protection materials

Because of the resemble properties observed in 2D materials, other 2D materials such as phosphorene (2D black phosphorus)<sup>122–130</sup> and molybdenum disulfide (MoS<sub>2</sub>)<sup>131</sup> were also studied for THz protection in recent research. Based on the SPPs and localized plasmon resonance in phosphorene, it was convenient to produce THz-absorbing MMs comprised of period structural phosphorene arrays. Wang *et al.*<sup>127</sup> designed ultra-wideband MMs by assembling dozens of phosphorene/dielectric pairs with different widths, in which the meta-

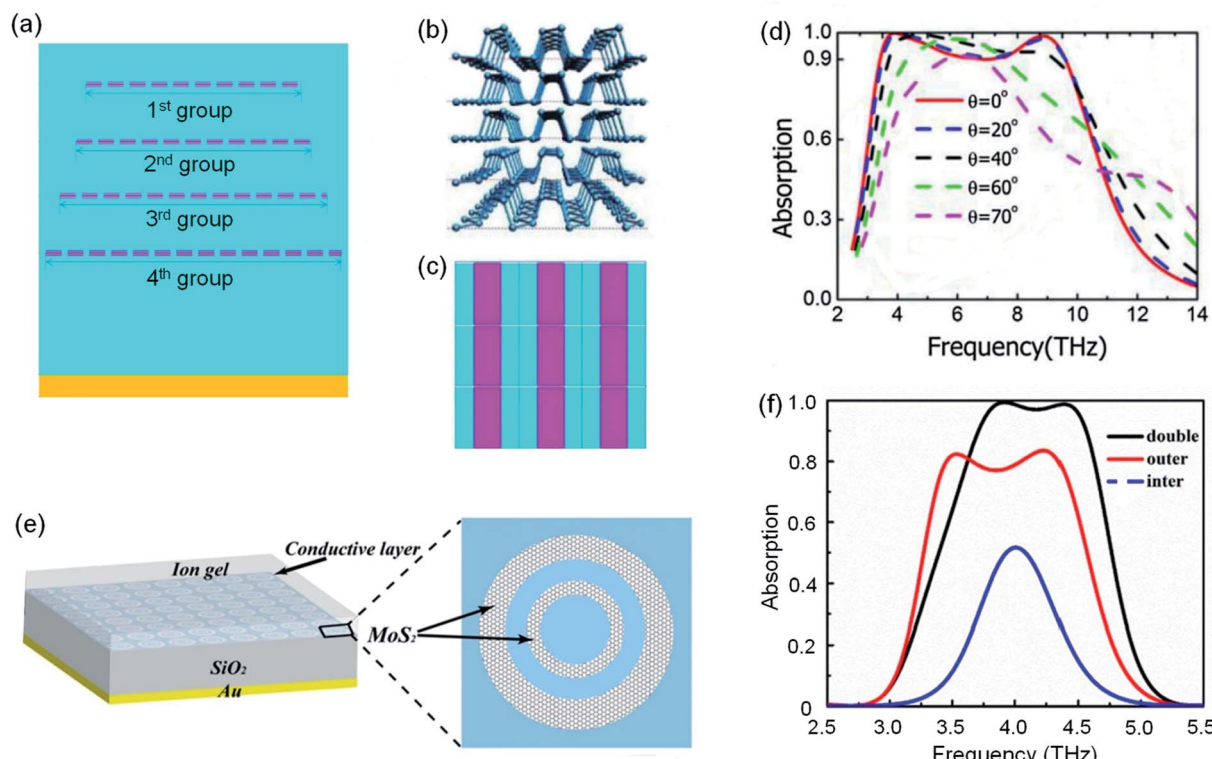


Fig. 12 (a) Unit cell, (b) structural details in each group, (c) top view across one phosphorene section and (d) THz absorption curves of phosphorene MMs (reproduced with permission from ref. 127 Copyright 2019 Springer Nature). (e) Schematic structure of the proposed THz-absorbing MMs comprising MCDRs and gold metal separated by a thin layer of silicon dioxide. (f) THz absorption curves of the designed MCDR absorber and MSR absorbers (reproduced with permission from ref. 131 Copyright 2019 Elsevier).



Table 1 Typical THz protection materials

Sample	Absorption	Effective bandwidth	Shielding effectiveness	Active control excitations	Ref.
Graphene/SiO <sub>2</sub> /p-Si/Au MMs	~0.8@620 GHz	—	—	Electric field	110
Graphene/polymer/Au MMs	0.95@0.5 THz, 0.97@1.5 THz	—	—	—	56
Porous graphene/cross-shape	0.96@1THz (TM), 0.97@0.87THz (TE)	—	—	Electric field	95
Au/liquid crystal/Au MMs	—	—	—	—	—
MXene/Au nano-slot MMs	—	—	20 dB@1.0 THz	—	13
Patterned graphene/PI/Au MMs	—	1.54–2.23 THz	—	—	108
Ion gel/graphene/stripe Al/PI/Al MMs	~20 dB@0.43 & 0.75 THz	—	—	Electric field	103
rGO paper	17.6 dB@0.7 THz	—	72.1 dB@ 0.6 THz	—	132
3D rGO foam	28 dB@1.6 THz	0.2–1.6 THz	28 dB@1.6 THz	Electric and optical field	10 and 36
WCNT/rGO foam	30 dB	1.5 THz (0.1–1.6 THz)	61 dB	—	33
Fe <sub>3</sub> O <sub>4</sub> /rGO foam	38 dB (average)	3.4 GHz–2.5 THz	—	—	35
MXene/rGO foam	30.6 dB (average)	0.2–2.0 THz	—	—	37
MXene/GO/Zn <sup>2+</sup> foam	—	0.86–2.0 THz	51 dB	—	16

structures were divided into 4 groups and distributed in 4 layers (Fig. 12a–c). The widths of the phosphorene stripes were identical in each group and different in distinct groups. Because of the asymmetrical structure and strong anisotropy, the simulated THz absorption results of the phosphorene MMs absorber showed that the absorption above 90% could cover 3.4–9.6 THz for normal incidence, while the absorber could retain high and ultra-wideband absorption within the incident angle of around 40° (Fig. 12d). In addition, as a typical 2D semiconductor with unique electrical, optical and magnetic properties, transition-metal dichalcogenides (MoS<sub>2</sub>) were also studied to design THz-absorbing MMs. Wang *et al.*<sup>131</sup> proposed angle-insensitive THz absorbing MMs composed of a monolayer MoS<sub>2</sub> concentric double ring (MCDR) metastructure and a metal film separated by a dielectric layer (Fig. 12e). For the plasma hybridization caused by the lateral coupling between the two separate MoS<sub>2</sub> rings, the THz absorption bandwidth and effectiveness could both be improved. Moreover, due to its special concentric structures, the absorber was insensitive to the incident angles and polarizations of the THz sources. Compared to the MoS<sub>2</sub> single ring (MSR) MMs with only separate outer or inner rings, the calculated results confirmed that the MCDRs absorber demonstrates obviously superior THz absorption in a wider THz waveband (Fig. 12f).

## 5. Summary and perspectives

With unique THz response characteristics, MM absorbers based on 2D materials in the forms of single layer, multiple layers, hybrid and tunable metasurfaces showed excellent THz absorbing performance. Recent advances in this field provided a sufficient theoretical and practical basis for THz protection, and the superior properties of 2D material MMs endow them with wide application prospects. However, due to the preparation limitations of the patterned 2D material metasurfaces, current research is mostly focused on theoretical designs and simulations, which has slowed the practical application of 2D material MMs. In addition, 3D intrinsic THz absorbing

materials based on porous or ordered 2D materials show exceptional THz protection performance; they effectively integrate the advantages of the intrinsic properties and structural characteristics of 2D materials. These special structures could optimize the surface impedance matching and form THz multiple scattering and electric transmission loss, which could realize high-efficiency absorption loss and active controllable protection performance in a wide THz waveband. Without considering the material thickness, 3D porous THz protection materials are more suitable for practical application in high-performance THz protection devices. Some typical THz protection materials and their performance are summarized and listed in Table 1.

The THz protection materials in future 6G applications should meet application requirements such as reduced dimensions, light weight, wide effective absorption bandwidth and high absorbing ability. Meanwhile, THz protection materials should also realize tunable THz protection performance. For THz protection MMs, the advances in nanomaterials science and nano-manufacturing technology should be adopted to realize enhanced THz protection and tunable characteristics of 2D materials, and the device integration fabrication ability should be fully considered to improve their performance in practical applications. For THz intrinsic protection materials, the influence of intrinsic properties (scale, defects, functional groups and flake sizes, *etc.*), inner nanostructures (hole structure or layer spacing, *etc.*) and doping behaviors with other loss materials (dielectric or magnetic particles, *etc.*) on the THz responses should be systematically studied.

## Conflicts of interest

There are no conflicts to declare.

## References

- 1 S. Dang, *et al.*, What should 6G be?, *Nat. Electron.*, 2020, 3(1), 20–29.



2 I. F. Akyildiz, J. M. Jornet and C. Han, Terahertz band: next frontier for wireless communications, *Phys. Commun.*, 2014, **12**, 16–32.

3 J. Federici and L. Moeller, Review of terahertz and subterahertz wireless communications, *J. Appl. Phys.*, 2010, **107**(11), 22.

4 D. M. Mittleman, Perspective: terahertz science and technology, *J. Appl. Phys.*, 2017, **122**(23), 230901.

5 T. J. Yen, *et al.*, Terahertz Magnetic Response from Artificial Materials, *Science*, 2004, **303**(5663), 1494.

6 H. Tao, *et al.*, A metamaterial absorber for the terahertz regime: design, fabrication and characterization, *Opt. Express*, 2008, **16**(10), 7181–7188.

7 Y. Zhang, *et al.*, Broadband and Tunable High-Performance Microwave Absorption of an Ultralight and Highly Compressible Graphene Foam, *Adv. Mater.*, 2015, **27**(12), 2049–2053.

8 B. Wen, *et al.*, Reduced Graphene Oxides: Light-Weight and High-Efficiency Electromagnetic Interference Shielding at Elevated Temperatures, *Adv. Mater.*, 2014, **26**(21), 3484–3489.

9 F. Shahzad, *et al.*, Electromagnetic interference shielding with 2D transition metal carbides (MXenes), *Science*, 2016, **353**(6304), 1137–1140.

10 Z. Huang, *et al.*, Ultra-Broadband Wide-Angle Terahertz Absorption Properties of 3D Graphene Foam, *Adv. Funct. Mater.*, 2018, **28**(2), 1704363.

11 M. Zdrojek, *et al.*, Graphene-based plastic absorber for total sub-terahertz radiation shielding, *Nanoscale*, 2018, **10**(28), 13426–13431.

12 H. H. Chen, *et al.*, Graphene-Based Materials toward Microwave and Terahertz Absorbing Stealth Technologies, *Adv. Opt. Mater.*, 2019, **7**(8), 16.

13 G. Choi, *et al.*, Enhanced Terahertz Shielding of MXenes with Nano-Metamaterials, *Adv. Opt. Mater.*, 2018, **6**(5), 1701076.

14 M. Amin, M. Farhat and H. Bağcı, An ultra-broadband multilayered graphene absorber, *Opt. Express*, 2013, **21**(24), 29938–29948.

15 M. Rahmanzadeh, H. Rajabalipanah and A. Abdolali, Multilayer graphene-based metasurfaces: robust design method for extremely broadband, wide-angle, and polarization-insensitive terahertz absorbers, *Appl. Opt.*, 2018, **57**(4), 959–968.

16 Z. Lin, *et al.*, Highly Stable 3D Ti3C2Tx MXene-Based Foam Architectures toward High-Performance Terahertz Radiation Shielding, *ACS Nano*, 2020, **14**(2), 2109–2117.

17 V. Bianchi, *et al.*, Terahertz saturable absorbers from liquid phase exfoliation of graphite, *Nat. Commun.*, 2017, **8**, 9.

18 L. F. Ye, *et al.*, Composite graphene-metal microstructures for enhanced multiband absorption covering the entire terahertz range, *Carbon*, 2019, **148**, 317–325.

19 N. I. Landy, *et al.*, Perfect Metamaterial Absorber, *Phys. Rev. Lett.*, 2008, **100**(20), 207402.

20 P. Yu, *et al.*, Broadband Metamaterial Absorbers, *Adv. Opt. Mater.*, 2019, **7**(3), 1800995.

21 G. Duan, *et al.*, A survey of theoretical models for terahertz electromagnetic metamaterial absorbers, *Sens. Actuators, A*, 2019, **287**, 21–28.

22 S. Liu and T. J. Cui, Concepts, Working Principles, and Applications of Coding and Programmable Metamaterials, *Adv. Opt. Mater.*, 2017, **5**(22), 1700624.

23 M. Kenney, *et al.*, Octave-Spanning Broadband Absorption of Terahertz Light Using Metasurface Fractal-Cross Absorbers, *ACS Photonics*, 2017, **4**(10), 2604–2612.

24 H. Tao, *et al.*, Highly flexible wide angle of incidence terahertz metamaterial absorber: design, fabrication, and characterization, *Phys. Rev. B: Condens. Matter Mater. Phys.*, 2008, **78**(24), 4.

25 N. I. Landy, *et al.*, Design, theory, and measurement of a polarization-insensitive absorber for terahertz imaging, *Phys. Rev. B: Condens. Matter Mater. Phys.*, 2009, **79**(12), 6.

26 M. Wu, *et al.*, A three-dimensional all-metal terahertz metamaterial perfect absorber, *Appl. Phys. Lett.*, 2017, **111**(5), 051101.

27 Q. H. Song, *et al.*, Liquid-metal-based metasurface for terahertz absorption material: frequency-agile and wide-angle, *APL Mater.*, 2017, **5**(6), 066103.

28 Z. H. Xu, *et al.*, Design of a Tunable Ultra-Broadband Terahertz Absorber Based on Multiple Layers of Graphene Ribbons, *Nanoscale Res. Lett.*, 2018, **13**, 8.

29 E. Galiffi, J. B. Pendry and P. A. Huidobro, Broadband Tunable THz Absorption with Singular Graphene Metasurfaces, *ACS Nano*, 2018, **12**(2), 1006–1013.

30 Z. Fei, *et al.*, Gate-tuning of graphene plasmons revealed by infrared nano-imaging, *Nature*, 2012, **487**(7405), 82–85.

31 R. J. Xu, X. Y. Liu and Y. S. Lin, Tunable ultra-narrowband terahertz perfect absorber by using metal-insulator-metal microstructures, *Results Phys.*, 2019, **13**, 102176.

32 Z. Song, *et al.*, Wide-angle absorber with tunable intensity and bandwidth realized by a terahertz phase change material, *Opt. Commun.*, 2020, **464**, 125494.

33 Z. Y. Huang, *et al.*, Graphene-Based Composites Combining Both Excellent Terahertz Shielding and Stealth Performance, *Adv. Opt. Mater.*, 2018, **6**(23), 9.

34 Z. Y. Huang, *et al.*, Research Progress on Terahertz Stealth and Shielding Materials, *Chem. J. Chin. Univ.*, 2019, **40**(6), 1103–1115.

35 H. Chen, *et al.*, Consecutively Strong Absorption from Gigahertz to Terahertz Bands of a Monolithic Three-Dimensional Fe3O4/Graphene Material, *ACS Appl. Mater. Interfaces*, 2019, **11**(1), 1274–1282.

36 S.-T. Xu, *et al.*, Active Terahertz Shielding and Absorption Based on Graphene Foam Modulated by Electric and Optical Field Excitation, *Adv. Opt. Mater.*, 2019, **7**(18), 1900555.

37 W. L. Ma, *et al.*, Compressible Highly Stable 3D Porous MXene/GO Foam with a Tunable High-Performance Stealth Property in the Terahertz Band, *ACS Appl. Mater. Interfaces*, 2019, **11**(28), 25369–25377.

38 A. Andryieuski and A. V. Lavrinenko, Graphene metamaterials based tunable terahertz absorber: effective



surface conductivity approach, *Opt. Express*, 2013, **21**(7), 9144–9155.

39 R.-M. Gao, *et al.*, Intensity-modulating graphene metamaterial for multiband terahertz absorption, *Appl. Opt.*, 2016, **55**(8), 1929–1933.

40 B. Wu, *et al.*, Experimental demonstration of a transparent graphene millimetre wave absorber with 28% fractional bandwidth at 140 GHz, *Sci. Rep.*, 2014, **4**(1), 4130.

41 R. Jadeja, *et al.*, Numerical investigation of graphene-based efficient and broadband metasurface for terahertz solar absorber, *J. Mater. Sci.*, 2020, **55**(8), 3462–3469.

42 K. Batrakov, *et al.*, Enhanced microwave-to-terahertz absorption in graphene, *Appl. Phys. Lett.*, 2016, **108**(12), 4.

43 Y. X. Zhou, *et al.*, Terahertz wave reflection impedance matching properties of graphene layers at oblique incidence, *Carbon*, 2016, **96**, 1129–1137.

44 D. D. Sun, *et al.*, Enhanced spatial terahertz modulation based on graphene metamaterial, *Chin. Opt. Lett.*, 2017, **15**(5), 4.

45 C. L. Cen, *et al.*, Plasmonic absorption characteristics based on dumbbell-shaped graphene metamaterial arrays, *Phys. E*, 2018, **103**, 93–98.

46 C. L. Cen, *et al.*, Tunable plasmonic resonance absorption characteristics in periodic H-shaped graphene arrays, *Superlattices Microstruct.*, 2018, **120**, 427–435.

47 C. Liu, L. M. Qi and X. Zhang, Broadband graphene-based metamaterial absorbers, *AIP Adv.*, 2018, **8**(1), 7.

48 C. L. Cen, *et al.*, Tunable absorption enhancement in periodic elliptical hollow graphene arrays, *Opt. Mater. Express*, 2019, **9**(2), 706–716.

49 Y. J. Li, *et al.*, Tunable quintuple-band polarization-insensitive wide-angle metasurface absorber with single-layered graphene in terahertz range, *Mater. Res. Express*, 2019, **6**(8), 8.

50 Z. M. Liu, L. Guo and Q. M. Zhang, A Simple and Efficient Method for Designing Broadband Terahertz Absorber Based on Singular Graphene Metasurface, *Nanomaterials*, 2019, **9**(10), 9.

51 Y. Qi, *et al.*, Tunable plasmonic absorber in THz-band range based on graphene “arrow” shaped metamaterial, *Results Phys.*, 2019, **15**, 102777.

52 S. Wu, *et al.*, Graphene-based single-layer elliptical pattern metamaterial absorber for adjustable broadband absorption in terahertz range, *Phys. Scr.*, 2019, **94**(10), 8.

53 D. X. Yan and J. S. Li, Tunable all-graphene-dielectric single-band terahertz wave absorber, *J. Phys. D: Appl. Phys.*, 2019, **52**(27), 7.

54 F. Chen, Y. Z. Cheng and H. Luo, A Broadband Tunable Terahertz Metamaterial Absorber Based on Single-Layer Complementary Gammadion-Shaped Graphene, *Materials*, 2020, **13**(4), 11.

55 B. Sensale-Rodriguez, *et al.*, Efficient terahertz electro-absorption modulation employing graphene plasmonic structures, *Appl. Phys. Lett.*, 2012, **101**(26), 3.

56 J. Min Woo, *et al.*, Graphene based salisbury screen for terahertz absorber, *Appl. Phys. Lett.*, 2014, **104**(8), 081106.

57 Z. Yi, *et al.*, Tunable Graphene-based Plasmonic Perfect Metamaterial Absorber in the THz Region, *Micromachines*, 2019, **10**(3), 11.

58 Y. Wang, *et al.*, Staked Graphene for Tunable Terahertz Absorber with Customized Bandwidth, *Plasmonics*, 2016, **11**(5), 1201–1206.

59 B. Xiao, M. Gu and S. Xiao, Broadband, wide-angle and tunable terahertz absorber based on cross-shaped graphene arrays, *Appl. Opt.*, 2017, **56**(19), 5458–5462.

60 J. G. Zhang, J. P. Tian and L. Li, A Dual-Band Tunable Metamaterial Near-Unity Absorber Composed of Periodic Cross and Disk Graphene Arrays, *IEEE Photonics J.*, 2018, **10**(2), 12.

61 Z. Yi, *et al.*, Tunable dual-band perfect absorber consisting of periodic cross-cross monolayer graphene arrays, *Results Phys.*, 2019, **13**, 102217.

62 K. Arik, S. AbdollahRamezani and A. Khavasi, Polarization Insensitive and Broadband Terahertz Absorber Using Graphene Disks, *Plasmonics*, 2017, **12**(2), 393–398.

63 R. Alaee, *et al.*, A perfect absorber made of a graphene micro-ribbon metamaterial, *Opt. Express*, 2012, **20**(27), 28017–28024.

64 Z. H. Zhu, *et al.*, Broadband single-layered graphene absorber using periodic arrays of graphene ribbons with gradient width, *Appl. Phys. Express*, 2015, **8**(1), 3.

65 S. Y. Xiao, *et al.*, Tunable light trapping and absorption enhancement with graphene ring arrays, *Phys. Chem. Chem. Phys.*, 2016, **18**(38), 26661–26669.

66 N. L. Mou, *et al.*, Hybridization-induced broadband terahertz wave absorption with graphene metasurfaces, *Opt. Express*, 2018, **26**(9), 11728–11736.

67 P. Kumar, A. Lakhtakia and P. K. Jain, Graphene pixel-based polarization-insensitive metasurface for almost perfect and wideband terahertz absorption, *J. Opt. Soc. Am. B*, 2019, **36**(8), F84–F88.

68 R. M. Gao, *et al.*, Graphene metamaterial for multiband and broadband terahertz absorber, *Opt. Commun.*, 2015, **356**, 400–404.

69 P. C. Wu, N. Papasimakis and D. P. Tsai, Self-Affine Graphene Metasurfaces for Tunable Broadband Absorption, *Phys. Rev. Appl.*, 2016, **6**(4), 8.

70 S. L. He and T. Chen, Broadband THz Absorbers With Graphene-Based Anisotropic Metamaterial Films, *IEEE Trans. Terahertz Sci. Technol.*, 2013, **3**(6), 757–763.

71 M. Faraji, M. K. Morawej-Farshi and L. Yousefi, Tunable THz perfect absorber using graphene-based metasurfaces, *Opt. Commun.*, 2015, **355**, 352–355.

72 Y. Q. Wang, *et al.*, Staked Graphene for Tunable Terahertz Absorber with Customized Bandwidth, *Plasmonics*, 2016, **11**(5), 1201–1206.

73 M. Chen, *et al.*, Frequency-tunable terahertz absorbers based on graphene metasurface, *Opt. Commun.*, 2017, **382**, 144–150.

74 S. Biabanifard, *et al.*, Tunable ultra-wideband terahertz absorber based on graphene disks and ribbons, *Opt. Commun.*, 2018, **427**, 418–425.



75 P. Fu, *et al.*, A broadband metamaterial absorber based on multi-layer graphene in the terahertz region, *Opt. Commun.*, 2018, **417**, 62–66.

76 R. Xing and S. S. Jian, A dual-band THz absorber based on graphene sheet and ribbons, *Opt. Laser Technol.*, 2018, **100**, 129–132.

77 R. Mishra, A. Sahu and R. Panwar, Cascaded Graphene Frequency Selective Surface Integrated Tunable Broadband Terahertz Metamaterial Absorber, *IEEE Photonics J.*, 2019, **11**(2), 2200310.

78 M. Soltani, *et al.*, A configurable two-layer four-bias graphene-based THz absorber, *J. Comput. Electron.*, 2020, **19**(2), 719–735.

79 G. S. Deng, *et al.*, Graphene-based tunable polarization sensitive terahertz metamaterial absorber, *Opt. Commun.*, 2016, **380**, 101–107.

80 E. S. Torabi, A. Fallahi and A. Yahaghi, Evolutionary Optimization of Graphene-Metal Metasurfaces for Tunable Broadband Terahertz Absorption, *IEEE Trans. Antennas Propag.*, 2017, **65**(3), 1464–1467.

81 Z. P. Wang and Y. M. Hou, Ultra-multiband absorption enhancement of graphene in a metal-dielectric-graphene sandwich structure covering terahertz to mid-infrared regime, *Opt. Express*, 2017, **25**(16), 19185–19194.

82 Y. T. Zhao, *et al.*, Switchable broadband terahertz absorber/reflector enabled by hybrid graphene-gold metasurface, *Opt. Express*, 2017, **25**(7), 7161–7169.

83 C. Shi, *et al.*, Investigation of graphene-supported tunable asymmetric terahertz metamaterials, *J. Opt. Soc. Am. B*, 2018, **35**(3), 575–581.

84 T. V. Huynh, *et al.*, Controlling the absorption strength in bidirectional terahertz metamaterial absorbers with patterned graphene, *Comput. Mater. Sci.*, 2019, **166**, 276–281.

85 L. Peng, *et al.*, Metal and graphene hybrid metasurface designed ultra-wideband terahertz absorbers with polarization and incident angle insensitivity, *Nanoscale Adv.*, 2019, **1**(4), 1452–1459.

86 L. M. Qi and C. Liu, Broadband multilayer graphene metamaterial absorbers, *Opt. Mater. Express*, 2019, **9**(3), 1298–1309.

87 M. R. Soheilifar and F. B. Zarrabi, Reconfigurable metamaterial absorber as an optical switch based on organic-graphene control, *Opt. Quantum Electron.*, 2019, **51**(5), 12.

88 X. M. Zhang, *et al.*, A Dual-Band Terahertz Absorber with Two Passbands Based on Periodic Patterned Graphene, *Materials*, 2019, **12**(18), 3016.

89 X. H. Deng, *et al.*, Tunable THz absorption in graphene-based heterostructures, *Opt. Express*, 2014, **22**(24), 30177–30183.

90 X. He, *et al.*, Investigation of graphene assisted tunable terahertz metamaterials absorber, *Opt. Mater. Express*, 2016, **6**(2), 331–342.

91 Q. H. Zhou, *et al.*, Controlling enhanced absorption in graphene metamaterial, *Opt. Commun.*, 2018, **413**, 310–316.

92 L. M. Qi, C. Liu and S. M. A. Shah, A broad dual-band switchable graphene-based terahertz metamaterial absorber, *Carbon*, 2019, **153**, 179–188.

93 A. Soleymani, R. E. Meymand and N. Granpayeh, Broadband near-perfect terahertz absorber in single-layered and non-structured graphene loaded with dielectrics, *Appl. Opt.*, 2020, **59**(9), 2839–2848.

94 H. Zhang, *et al.*, A water hybrid graphene metamaterial absorber with broadband absorption, *Opt. Commun.*, 2020, **463**, 125394.

95 L. Wang, *et al.*, Graphene-assisted high-efficiency liquid crystal tunable terahertz metamaterial absorber, *Opt. Express*, 2017, **25**(20), 23873–23879.

96 Y. C. Fan, *et al.*, Broadband Terahertz Absorption in Graphene-Embedded Photonic Crystals, *Plasmonics*, 2018, **13**(4), 1153–1158.

97 B.-z. Xu, *et al.*, A novel structure for tunable terahertz absorber based on graphene, *Opt. Express*, 2013, **21**(20), 23803–23811.

98 Y. Zhang, *et al.*, Graphene based tunable metamaterial absorber and polarization modulation in terahertz frequency, *Opt. Express*, 2014, **22**(19), 22743–22752.

99 X. He, *et al.*, Active graphene metamaterial absorber for terahertz absorption bandwidth, intensity and frequency control, *Opt. Mater. Express*, 2018, **8**(4), 1031–1042.

100 X. Huang, *et al.*, Polarization-independent and angle-insensitive broadband absorber with a target-patterned graphene layer in the terahertz regime, *Opt. Express*, 2018, **26**(20), 25558–25566.

101 Y. Jiang, *et al.*, Design and performance of a terahertz absorber based on patterned graphene, *Opt. Lett.*, 2018, **43**(17), 4296–4299.

102 L. Qi, C. Liu and S. M. A. Shah, A broad dual-band switchable graphene-based terahertz metamaterial absorber, *Carbon*, 2019, **153**, 179–188.

103 X. Chen, *et al.*, Electrically Tunable Perfect Terahertz Absorber Based on a Graphene Salisbury Screen Hybrid Metasurface, *Adv. Opt. Mater.*, 2020, **8**(3), 1900660.

104 X. Jin, *et al.*, Coherent perfect absorber with independently tunable frequency based on multilayer graphene, *Opt. Commun.*, 2019, **446**, 44–50.

105 Z. Xu, *et al.*, Design of a Tunable Ultra-Broadband Terahertz Absorber Based on Multiple Layers of Graphene Ribbons, *Nanoscale Res. Lett.*, 2018, **13**(1), 143.

106 M. Y. Gu, B. G. Xiao and S. S. Xiao, Tunable THz perfect absorber with two absorption peaks based on graphene microribbons, *Micro Nano Lett.*, 2018, **13**(5), 631–635.

107 X. J. He, *et al.*, Active graphene metamaterial absorber for terahertz absorption bandwidth, intensity and frequency control, *Opt. Mater. Express*, 2018, **8**(4), 1031–1042.

108 Y. Jiang, *et al.*, Design and performance of a terahertz absorber based on patterned graphene, *Opt. Lett.*, 2018, **43**(17), 4296–4299.

109 S. H. Lee, *et al.*, Switching terahertz waves with gate-controlled active graphene metamaterials, *Nat. Mater.*, 2012, **11**(11), 936–941.



110 B. Sensale-Rodriguez, *et al.*, Extraordinary Control of Terahertz Beam Reflectance in Graphene Electro-absorption Modulators, *Nano Lett.*, 2012, **12**(9), 4518–4522.

111 R. Cheng, *et al.*, Tunable graphene-based terahertz absorber via an external magnetic field, *Opt. Mater. Express*, 2020, **10**(2), 501–512.

112 M. B. Heydari and M. H. V. Samiei, An Analytical Study of Magneto-Plasmons in Anisotropic Multi-layer Structures Containing Magnetically Biased Graphene Sheets, *Plasmonics*, 2020, **16**.

113 A. C. Tasolamprou, *et al.*, Experimental Demonstration of Ultrafast THz Modulation in a Graphene-Based Thin Film Absorber through Negative Photoinduced Conductivity, *ACS Photonics*, 2019, **6**(3), 720–727.

114 S. Borzooei, E. Rezagholizadeh and M. Biabanifard, Graphene disks for frequency control of terahertz waves in broadband applications, *J. Comput. Electron.*, 2020, **19**(2), 759–772.

115 J. S. Li, *et al.*, Flexible electromagnetic wave absorbing composite based on 3D rGO-CNT-Fe<sub>3</sub>O<sub>4</sub> ternary films, *Carbon*, 2018, **129**, 76–84.

116 Z. Huang, *et al.*, Graphene-Based Composites Combining Both Excellent Terahertz Shielding and Stealth Performance, *Adv. Opt. Mater.*, 2018, **6**(23), 1801165.

117 G. Li, *et al.*, Dynamical Control over Terahertz Electromagnetic Interference Shielding with 2D Ti<sub>3</sub>C<sub>2</sub>Ty MXene by Ultrafast Optical Pulses, *Nano Lett.*, 2020, **20**(1), 636–643.

118 K. Hantanasirisakul and Y. Gogotsi, Electronic and Optical Properties of 2D Transition Metal Carbides and Nitrides (MXenes), *Adv. Mater.*, 2018, **30**(52), 1804779.

119 H. Wang, *et al.*, Clay-Inspired MXene-Based Electrochemical Devices and Photo-Electrocatalyst: State-of-the-Art Progresses and Challenges, *Adv. Mater.*, 2018, **30**(12), 1704561.

120 T. Yun, *et al.*, Electromagnetic Shielding of Monolayer MXene Assemblies, *Adv. Mater.*, 2020, **32**(9), 9.

121 Y. I. Jhon, M. Seo and Y. M. Jhon, First-principles study of a MXene terahertz detector, *Nanoscale*, 2018, **10**(1), 69–75.

122 Y. M. Qing, H. F. Ma and T. J. Cui, Tailoring anisotropic perfect absorption in monolayer black phosphorus by critical coupling at terahertz frequencies, *Opt. Express*, 2018, **26**(25), 32442–32450.

123 X. Wang, *et al.*, Tunable terahertz/infrared coherent perfect absorption in a monolayer black phosphorus, *Opt. Express*, 2018, **26**(5), 5488–5496.

124 D. X. Dong, *et al.*, Tunable THz reflection-type polarizer based on monolayer phosphorene, *Appl. Opt.*, 2019, **58**(35), 9643–9650.

125 Y. N. Jiang, *et al.*, Broadband linear-to-circular polarization converter based on phosphorene metamaterial, *Opt. Mater. Express*, 2019, **9**(5), 2088–2097.

126 G. Tianjing and C. Argyropoulos, Polarization-Independent and Broadband THz Coherent Perfect Absorber based on Black Phosphorus Bifacial Metasurfaces, in *2019 IEEE International Symposium on Antennas and Propagation and USNC-URSI Radio Science Meeting*, 2019, IEEE, pp. 567–568.

127 J. Wang and Y. N. Jiang, A phosphorene-based metasurface absorber operating in ultra-wideband terahertz regime, *Eur. Phys. J. D*, 2019, **73**(12), 255.

128 Y. J. Cai, *et al.*, Investigation of multi-resonant and anisotropic plasmonic resonances in the stacked graphene-black phosphorus bilayers, *J. Phys. D: Appl. Phys.*, 2020, **53**(2), 025107.

129 T. T. Liu, *et al.*, Tunable anisotropic absorption in monolayer black phosphorus using critical coupling, *Appl. Phys. Express*, 2020, **13**(1), 5.

130 W. Tongling, *et al.*, Tunable broadband terahertz metamaterial absorber using multi-layer black phosphorus and vanadium dioxide, *J. Phys. D: Appl. Phys.*, 2020, **53**(14), 145105.

131 X. Y. Wang, *et al.*, Angle insensitive broadband terahertz wave absorption based on molybdenum disulfide metamaterials, *Superlattices Microstruct.*, 2019, **135**, 5.

132 S. Dong, *et al.*, Flexible reduced graphene oxide paper with excellent electromagnetic interference shielding for terahertz wave, *J. Mater. Sci.: Mater. Electron.*, 2018, **29**(20), 17245–17253.

